AIAA SciTech
5-9 January 2015, Kissimmee, Florida
AIAA Modeling and Simulation Technologies Conference

Design and Evaluation of a Semi-Empirical Piece-wise Exponential Atmospheric Density Model for CubeSat Applications

Siddharth S. Kedare* and Steve Ulrich†
Carleton University, Ottawa, Ontario K1S 5B6, Canada

This paper presents the theory and design of a semi-empirical atmospheric density model based on data from the MSIS-86 model. Created as part of ongoing research into optimal guidance laws for nanosatellite applications, this model focuses on being computationally lightweight, while providing reasonably accurate atmospheric density predictions at geometric altitudes ranging from 0 - 1000 km. The model is validated against data from existing analytical and empirical atmospheric models. It is then implemented in a variety of orbit and attitude propagation environments in Matlab-Simulink to assess its stability, validity, and computational footprint. The orbital elements from each simulation were compared against those obtained from baseline simulations run using the Naval Research Lab (NRL) MSISE-00 model. The results show good agreement with the baseline simulations, while indicating a significant reduction in computational run time.

I. Introduction

Recent advances in nanosatellite technology and mobile computing have provided the potential for increased availability of on-orbit computing power. In 2013, STRaND-1 was launched into orbit, carrying a classic CubeSat computer and a Google Nexus One smartphone.[1] Additionally, as part of the Small Spacecraft Technology Program, NASA has launched five PhoneSats into Low Earth Orbit (LEO), the most recent in April 2014 aboard a SpaceX Falcon IX launch vehicle.[2] These missions demonstrated the ability to successfully incorporate smartphone technology into CubeSats, and presented a significant advancement over existing CubeSat processors such as the ISIS OBC, which is built around an ARM9 architecture clocked at 400 MHz.[3]

The improvements in processing capability open up the potential for the inclusion of on-board orbit and attitude propagation systems. Such a system has been previously designed,[4] but requires frequent ground-based updates as it neglects perturbation effects in an effort to minimize computational cost. However, real-time knowledge of these perturbations and their effects - through on-board orbit and attitude propagation - could prove valuable for science missions, low-cost Earth observation platforms, and spacecraft guidance systems. For example, a 3U CubeSat could autonomously predict an increase in atmospheric drag, and plan a maneuver to reorient itself so as to minimize orbital decay. Nevertheless, from a scientific perspective, the CubeSat payloads should have computational priority, and it is therefore desirable to minimize the processing power necessary for GN&C operations, while including any major perturbation effects.

These perturbing accelerations constantly affect the attitude and orbit of a satellite, and include atmospheric drag, Earth oblateness, luni-solar gravitational forces, and solar radiation pressure. As presented by Montenbruck and Gill,[5] atmospheric drag and Earth oblateness are the dominant perturbing factors in LEO. The spherical harmonic geopotential model provides accurate data on the gravitational perturbations due to Earth oblateness. In its simplest form, accounting for J_{20} perturbations, it is only marginally more complex than a basic two-body Keplarian propagator.[6] A large number of atmospheric drag models are available in the literature, however they are not adequate for implemention into nanosatellites as most of them re-

*M.A.Sc Candidate, Department of Mechanical and Aerospace Engineering, 1125 Colonel By Drive. Student Member AIAA.
†Assistant Professor, Department of Mechanical and Aerospace Engineering, 1125 Colonel By Drive. Member AIAA.

quire multiple inputs, extensive lookup tables, and numerical integration, which make them computationally complex.

This paper focuses on the development and validation of a low computation atmospheric density model, named SPeAD-M86, for CubeSat applications. This document is organized as follows: Section II discuses the importance of atmospheric density on drag perturbation calculation, and presents the most-widely used existing atmospheric models. Section III formally defines the approach and implementation of the SPeAD-M86 model. Section IV details the validation procedures for determining the accuracy, stability, and performance of the SPeAD-M86 model. In Section V, results from the SPeAD-M86 model are compared with published empirical atmospheric data. In addition, results from the validation routines are presented.

II. Current Analytical and Empirical Models

Atmospheric drag is the primary nongravitational force acting on satellites in LEO.[7] Acting opposite to the velocity vector, it removes energy from an orbit, reducing the semi-major axis and the eccentricity,[8] leading to the eventual reentry of the spacecraft. The acceleration due to drag is given by

$$\ddot{\vec{r}}_{drag} = -\frac{1}{2} C_D \frac{A}{m} \rho |\vec{v_r}| \vec{v_r} \tag{1a}$$

where

$$A = \sum_{i=1}^{n} A_n \begin{cases} A_n = 0, & \text{if } \vec{A}_n \cdot \vec{v_r} < 0. \\ A_n = \vec{A}_n \cdot \vec{v_r} & \text{otherwise.} \end{cases} \tag{1b}$$

where m is the spacecraft mass, C_D is the drag coefficient, A is the total projected area perpendicular to $\vec{v_r}$, $\vec{A}_n$ is the area vector for the n^{th} spacecraft panel in the body frame, ρ is the atmospheric density, and $\vec{v_r}$ is the velocity of the spacecraft relative to the atmosphere. Similarly, the torque acting on a spacecraft due to atmospheric drag can be expressed as

$$\vec{T}_{drag} = \sum_{i=1}^{n} \vec{F}_{drag_i} \times \vec{r}_{cp_i} \tag{2}$$

where $\vec{F}_{drag_i}$ is the drag force acting on each spacecraft panel, and $\vec{r}_{cp_i}$ is the center of pressure location of each spacecraft panel in the body frame. m is typically known for a spacecraft, while A can be calculated from knowledge of the spacecraft geometry, velocity $\vec{v_r}$, and the spacecraft attitude state.[9] Similarly, for the torque equation, $\vec{r}_{cp_i}$ is based on the satellite geometry. The spacecraft drag coefficient, C_D, is a difficult parameter to determine, due to the complex interaction of spacecraft geometry, reflection, molecular content, and spacecraft attitude.[10] Typically, for continuum flows, C_D is in the range of 2 - 4. Vallado and Finkleman[11] provide an overview of research into spacecraft drag coefficient determination. For the purposes of this study, a C_D of 2.2 was selected, corresponding to the free molecular regime as defined by Montenbruck and Gill[5] The atmospheric density ρ however is dependent on the satellite position, and is not easily predictable as it varies nonlinearly, by orders of magnitude, with altitude. Numerous atmospheric models have been developed and revised over the years; these shall now be briefly discussed.

II.A. Simple Exponential

The exponential relation of density with altitude is apparent from data published in standard and reference atmospheres.[12] Therefore, as a first approximation, an exponential relation dependent on the geometric altitude can be defined.

$$\rho = \rho_0 \exp\left[\frac{-(z - h_0)}{H}\right] \tag{3}$$

where ρ is the density at any altitude, ρ_0 is the density at some specified base altitude h_0, H is the scale height at h_0, and z is the spacecraft altitude above sea level. The scale height is defined as the height over which the atmospheric pressure drops to e^{-1} of that at the base altitude. Such a model, based on Vallado,[13] was implemented during ground testing of the PROBA 1 and 2 spacecraft GN&C systems. Though simple, this model is constrained to a small altitude range to remain accurate, and therefore cannot be utilized for real-time orbital and attitude propagation on-board nanosatellites in high eccentricity orbits.

II.B. Harris-Priester

The Harris-Priester model is based on upper atmosphere data derived from the heat conduction equation. It accounts for the daily temperature variations in the atmosphere by means of a cosine variation. Presented below is the general expression for the Harris-Priester model.[5,14]

$$\rho(z) = \rho_m(h) + [\rho_M(h) - \rho_m(h)] \cdot cos^n \left(\frac{\Psi}{2}\right) \tag{4}$$

where $\rho_m(h)$ and $\rho_M(h)$ are piece-wise functions of the Harris-Priester atmospheric density coefficients at specified altitude intervals and the spacecraft altitude z, n is dependent on the orbit inclination, and Ψ is the angle between the position of the spacecraft to the density peak. Calculating this angle requires data on the sun's location with respect to the spacecraft, which is not always readily available on CubeSats.

II.C. Jacchia 1971

L.G. Jacchia published a number of empirical density models, which evolved between 1965 and 1977. Initially focused on geodetic height and temperature as the parameters, these models eventually provided density variations as a function of time. The Jacchia 1971 (J71) model provides time-variant atmospheric density between altitudes of 90-2500 km.[15] This model does however require numerical integration, making it computationally intensive to implement.

II.D. Jacchia-Roberts

Robert's method is based on the analytical solutions of the barometric and diffusion differential equations obtained by integration of the governing partial differential equations. Derived from the J71 model, the results closely agree with Jacchia for altitudes above 125 km. Furthermore, Robert's model eliminates the need for numerical integration, improving computational speed.[16]

II.E. CIRA 1972

The COSPAR International Reference Atmosphere (CIRA) is an empirical model of atmospheric temperature and density from 0 - 2000 km. It combines mean data from 25 - 500 km, obtained from satellite drag measurements and ground observations, with J71 data from 110 - 2000 km.[17] CIRA has been periodically updated as new data is obtained, most recently in 1986.

II.F. 1976 US Standard Atmosphere

As a result of extensive rocket data and revised theories for the upper atmosphere, the existing 1962 US Standard Atmosphere was updated and published in a joint effort between NOAA, NASA and the USAF.[18] Atmospheric properties up to 1000 km altitude based on mid-latitude measurements are tabulated, requiring the storage and use of large lookup tables.

II.G. Jacchia-Bowman 2008

The Jacchia-Bownman 2008 (JB-2008) model is an empirical, thermospheric density model, developed to improve upon the JB-2006 model, which was developed from the CIRA 1972 model diffusion equations.[19] The modifications implement new exospheric temperature and semi-annual density equations, factor in geomagnetic storm effects, and include updated solar indices.

II.H. Mass Spectrometer Incoherent Scatter

NASA Goddard Space Flight Center developed several empirical neutral atmospheric models, referred to as the Mass Spectrometer Incoherent Scatter (MSIS) model class, based on mass spectrometer and incoherent radar scatter data from satellite and ground measurements. Inputs to the model, are year, day of year, universal time, altitude, geodetic latitude and longitude, local apparent solar time, solar $F_{10.7}$ flux and geomagnetic index. The MSIS-86 model constitutes the upper part of the CIRA-1986.[20] In 1990, MSIS-86 was subsequently revised in the lower thermosphere and extended into the mesosphere and lower atmosphere to provide a single analytic model refered to as MSIS-90.[21]

II.I. NRLMSISE-00

This model, developed by the Naval Research Laboratory (NRL), incorporates data collected since the MSIS-86 and MSIS-90 models, and improves upon them by accounting for atomic oxygen, revising molecular consituents in the lower atmosphere and adding further nonlinear terms to account for the effects of solar activity.[22]

III. Theory and Design of the SPeAD-M86 Model

Though the majority of the atmospheric density models discussed in Section II have been used previously for ground-based precision orbit determination, they require large lookup tables or multiple inputs in addition to spacecraft altitude. For potential CubeSat applications, minimizing computational storage and processing requirements while maintaining reasonable accuracy is critical. Therefore, it is essential to develop a simplified model which closely follows published data from existing models while striving for a minimal computational footprint.

III.A. Piece-wise Exponential Density Model

The simple exponential model, though severely limited by its inability to account for variable solar flux and geomagnetic effects in real time, offers a computationally inexpensive correlation between altitude and density. As previously mentioned, it fails to maintain accuracy over a large range of altitudes. Vallado and McClain,[13] and Walter[14] provide insight into the piece-wise exponential approach as an alternative formulation. It draws on similarities with the Harris-Priester model.

$$\rho = \rho_i \exp\left[\frac{-(z-h_i)}{H_i}\right] \quad @ \quad h_i < z < h_{(i+1)} \tag{5}$$

where z is the geometric altitude above sea level, h_i are the base altitudes for a given altitude interval, ρ_i is the corresponding base density, and H_i is the scale height applicable for the interval. The model provided by Vallado and McClain[13] was accompanied by a lookup table calibrated against the CIRA72 model. For completeness, this model was implemented, and found to be insufficient at providing a continuous density formulation. Results illustrating this are presented in Section V. Table 3 in the appendix contains the associated altitude interval data.

III.B. Calibration against the MSIS-86 model

The accuracy of a piece-wise approximation is dictated by the empirical model against which it is calibrated. Given the outdated nature of CIRA72, and the desire to obtain a model which best reflects the mean density, MSIS-86 atmospheric data and scale heights tabulated by Wertz and Larson[7] were used for the calibration. An MSIS model was selected for the calibration data set as it demonstrates slight improvements over the Jacchia models.[23] The data are averaged across the Earth with a 30° step size in longitude and a 20° step size in latitude. All data were for a mean solar flux $F_{10.7} = 118.7 \times 10^{-22}$ W·m^{-2}·Hz^{-1}. Density data corresponding to a maximum and minimum $F_{10.7}$ were not included in the calibration process, but are included in the results for comparison purposes. To allow for a better curve fit with the existing MSIS data, the scale heights were modified for an altitude below 150km. Furthermore, at altitudes above 1000 km, the density is set to zero. This proposed version of the existing piece-wise model is hereafter referred to as the SPeAD-M86b model, indicating the use of a baseline altitude. Columns 1-3 of Table 4 contain the interval data employed during this calibration.

III.C. Reduction of Variable Dependence

In an effort to further simplify the density model, and reduce the number of lookup variables, the piece-wise exponential model was reduced to be solely dependent on the altitude above sea level, by eliminating the base height lookup variable. This approach led to the base density being redefined as a *scale density*, which does not necessarily correspond to the density at the beginning of an altitude interval.

$$\rho = \rho_{s_i} \exp\left(\frac{-z}{H_i}\right) \quad @ \quad h_i < z < h_{(i+1)} \tag{6}$$

where ρ_s is the scale density for a given altitude interval, while z and H_i are identical as defined earlier in Eq. (5). A similar formulation for an isothermal model of planetary atmospheres, often employed by planetary probes, is presented by Tewari.[24] Using this reduced variable dependence required re-calibration of the model to find ρ_s for each altitude interval. The calibration was performed so as to minimize discontinuities in the density between intervals. This version of the piece-wise model is hereafter referred to as the SPeAD-M86 model. Table 4 in the appendix presents the interval data employed during this calibration.

IV. Validation Routines

To validate the SPeAD-M86 model, it was necessary to compare the computed density with published empirical and analytic atmospheric density data. Empirical data was obtained from the MSIS-86[7] and JB-2008[25] at the average, maximum, and minimum $F_{10.7}$, 1976 US Standard Atmosphere,[12] mean CIRA-86,[12] and NRLMSISE-00 at equatorial latitude averaged over diurnal and seasonal variations.[25] Data points from empirical sources were obtained by digitizing of the relevant graphics. The SPeAD-M86 model results were also compared against the CIRA72 piece-wise,[13] simple exponential, and SPeAD-M86b analytical models. The altitude step size for all analytical models was 5 km and the modulus of the relative error was calculated using the equation below.

$$\%error = \frac{|\rho_a - \rho|}{\rho_a} * 100\% \tag{7}$$

where ρ is the atmospheric density calculated by SPeAD-M86, and ρ_a is the density from each of the other three analytical models. This equation quantifies the variation of the SPeAD-M86b, CIRA72, and simple exponential models from the SPeAD-M86 model.

In addition to direct density comparisons, the stability and accuracy of the model was verified in an orbit and attitude propagator implemented using the MATLAB-Simulink environment. A 3U CubeSat in LEO with no active control system was considered for this study. The initial classical orbital elements of the satellite with respect to Earth were defined as follows.

$$[a_0 \quad e_0 \quad i_0 \quad \Omega_0 \quad \omega_0 \quad \nu_0] = [6878 \text{ km} \quad 0.05 \quad 0.1^\circ \quad 270^\circ \quad 90^\circ \quad 0^\circ]$$

The elements correspond to a 156.1 km × 843.9 km orbit having a period of 94.6 minutes, with a low inclination of 0.1° to the equatorial plane of the Earth. Such an "atmosphere grazing" orbit could result from a failed circularization burn by the launch/deployment vehicle. Though unlikely for a CubeSat, it provides a scenario in which the atmospheric drag has a significant effect on the spacecraft near perigee. Furthermore, it allows the SPeAD-M86 model to be evaluated over a range of altitudes. To obtain consistent and unbiased results, it was necessary to implement the model in a variety of simulation environments. For each environment, the time variation of the orbital elements using the SPeAD-M86 model was compared with the variation computed using the NRLMSISE-00 model available in Simulink. The NRLMSISE-00 model was selected as a baseline as it has been recommended by NASA to become the standard for use in satellite orbit prediction.[22,26] Table 1 presents the simulation environments utilized for validation, along with the variable parameters. All of the environments included the effects of gravity gradient torque, atmospheric drag, and atmospheric torque, while utilizing the ode3 (Bogacki-Shampine) integrator for orbit propagation over a simulation time of 86,400 seconds.

Parameter	Environment A	Environment B	Environment C	Environment D
Time step, Δt (sec)	0.1	0.1	1.0	1.0
Gravity model type	Spherical	Zonal	Spherical	Zonal
Order of gravity model	8	2	8	2
Attitude propagation	Quaternion EoM	STM	Quaternion EoM	STM
Attitude integrator	ode3	Forward Euler	ode3	Forward Euler

Table 1: Summary of Simulation Environments

Environment A models the perturbations in LEO to a high degree of accuracy, while B is a simplified model designed to reduce CPU run-time. A State Transition Matrix (STM) technique, as presented by Whitmore,[27] was implemented for attitude propagation in B and D, thereby reducing the number of continuous

integrations necessary. This was expected to reduce CPU run time, the results of which discussed further in Section V.C. The forward Euler integration was not implemented into the orbit propagator due to observed instability and sensitivity to initial conditions. Environments C and D are identical to A and B respectively, differing only by the use of a larger time step. All were run on a single logical thread of an Intel®Core™ i7 2700K 3.9 GHz processor with 8 GB available memory.

Geomagnetic index data, required as an input for the NRLMSISE-00 model, was taken from NOAA[28] for January 4, 2014. Average solar flux index $F_{10.7a}$ and daily solar flux index $F_{10.7}$ data was obtained for May 15, 2014 as observed and derived from the GPS IONO model.[29] In addition, anomalous oxygen calculations were switched on for the NRLMSISE-00 model.

The orbital element error for the first five (a, e, i, Ω, ω) was calculated as a percentage error using the NRLMSISE-00 data as the baseline. However, due to the cyclic nature of ν from 0 to 2π rad., such a quantification would not provide a clear representation of the actual error. Instead, the smallest difference in ν at each time step was calculated, and normalized against a full orbit (i.e. 2π rad). The MATLAB code for this error formulation is included in the Appendix. In addition to examining the accuracy and sensitivity of the SPeAD-M86 model, it was essential to quantify and compare the CPU run time against a NRLMSISE-00 baseline. The run times were obtained using the `tic - toc` functions in MATLAB, and averaged over 10 simulation runs per model in each environment.

V. Simulation Results

This section summarizes the results of the validation routines outlined in Sec. IV. Note that the actual orbital elements for each density model-simulation environment combination are not directly relevant towards the validation of the SPeAD-M86 model, but are included in the appendix for completeness.

V.A. Comparison with Empirical Data

Figure 1 presents the SPeAD-M86 model alongside published density data from several empirical models.

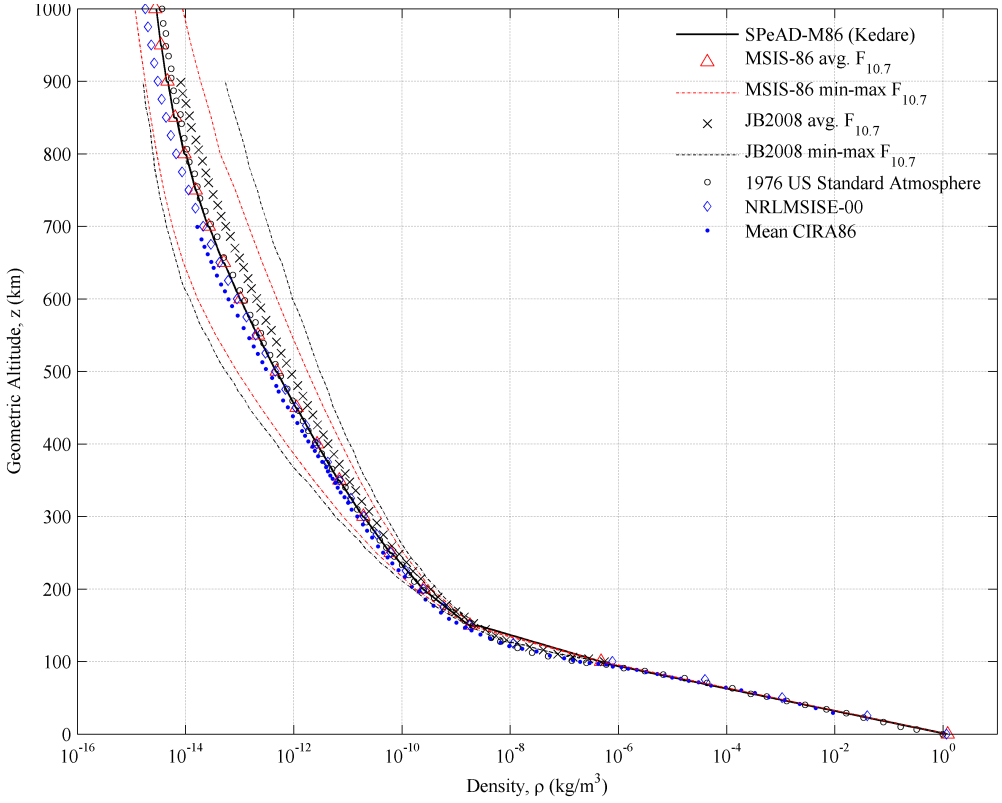

Figure 1. Comparison of SPeAD-M86 data against published empirical atmospheric density data.

As illustrated, the SPeAD-M86 data closely matches published empirical data from a number of models. The SPeAD-M86 data passes approximately halfway between the minimum and maximum density estimate boundaries provided by the MSIS-86 and JB2008 models. It therefore provides a good one-to-one approximation of the mean density. The even scatter of empirical data points about the SPeAD-M86 dataset is an indicator of a good correlation with previously observed atmospheric conditions. Between 100 km and 150 km, a minor deviation from published data is observed, with the SPeAD-M86 model slightly overpredicting the density. However, without continuous propulsive maneuvers below an altitude of 150 km, atmospheric drag rapidly decays the orbit of a satellite. Useful CubeSat orbits are typically higher than this altitude, and thus the departure from published data is not considered to diminish the overall usefulness of the model. However, as a result of this discrepancy, care should be taken to ensure the model is not utilized for atmospheric re-entry predictions.

Figure 2 presents the density variation between the SPeAD-M86 model and other analytical models. Due to the close empirical agreement of the SPeAD-M86 model presented in Figure 1, the error graph provides an estimate of the error between these models and published empirical data.

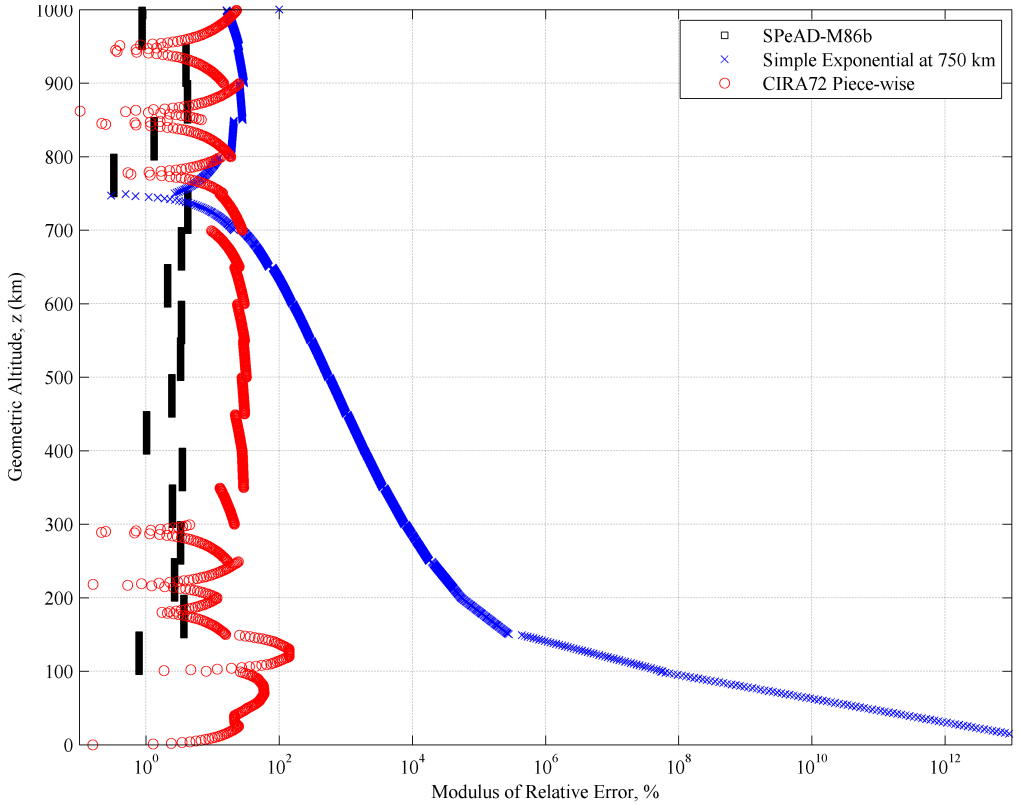

Figure 2. Relative error of select analytical models against SPeAD-M86 data.

The variation of the SPeAD-M86b model is less than 10% for the entire altitude range under consideration, which was anticipated as it used the same calibration data set as the final SPeAD-M86 model. The CIRA72 piece-wise model deviates significantly from the SPeAD-M86 model, with the error varying between 1% and 60% for the majority of altitudes. Between 300 km and 700 km, the CIRA72 model exhibits a severe deviation from the SPeAD-M86 baseline. It is only at altitudes above 750 km that it provides an acceptable estimate of density. The simple exponential model herein, designed specifically for an altitude of $\approx$ 750 km, exhibits a very large relative errors for altitudes below 725 km and above 775 km. Therefore, this model, though extremely simple, would not provide useful estimates of atmospheric density in orbits with significant eccentricity.

V.B. Orbital Element Error

The orbital elements were obtained from the each simulation environment, and a comparison made between the SPeAD-M86 and NRLMSISE-00 implementations, with the latter used as the baseline. Figure 3 presents the error between the orbital elements for SPeAD-M86 and NRLMSISE-00 implementations in Environment A.

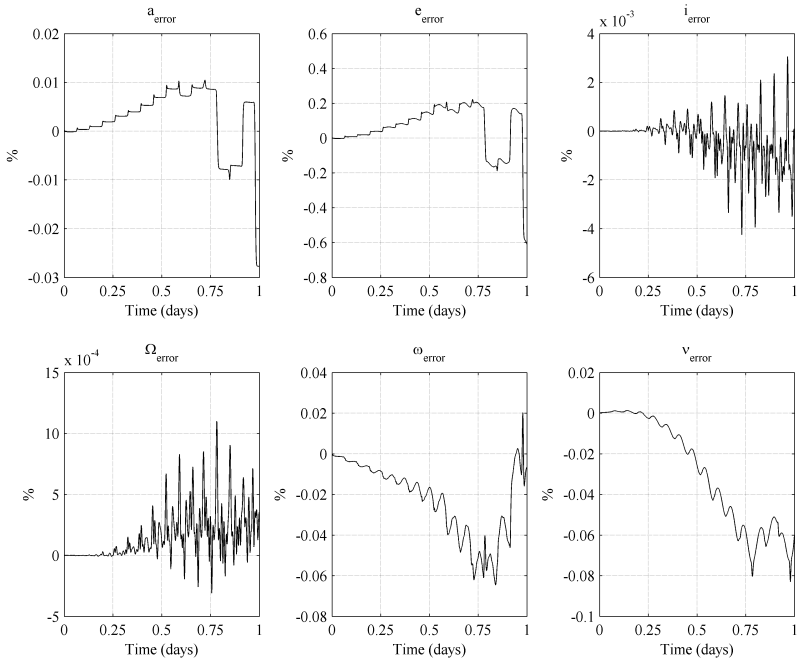

Figure 3. Environment A: Orbital element error between SPeAD-M86 and NRLMSISE-00 implementation.

The largest orbital element error is less than 1% for the duration of the simulation, and the elements relating to the shape of the orbit (a, e) show good correlation with the NRLMSISE-00 implementation. The elements relating to the orientation of the orbit (i, Ω, ω) also appear to closely follow the NRLMSISE-00 baseline. The error appears to increase in an oscillatory manner over time, particularly for i and Ω. Finally, the location of the spacecraft in the orbit, ν, shows an error of less than 0.1%. An examination of the time variant density from both atmospheric models, presented in Figure 4 and 5, provides further insight into the source of these small errors.

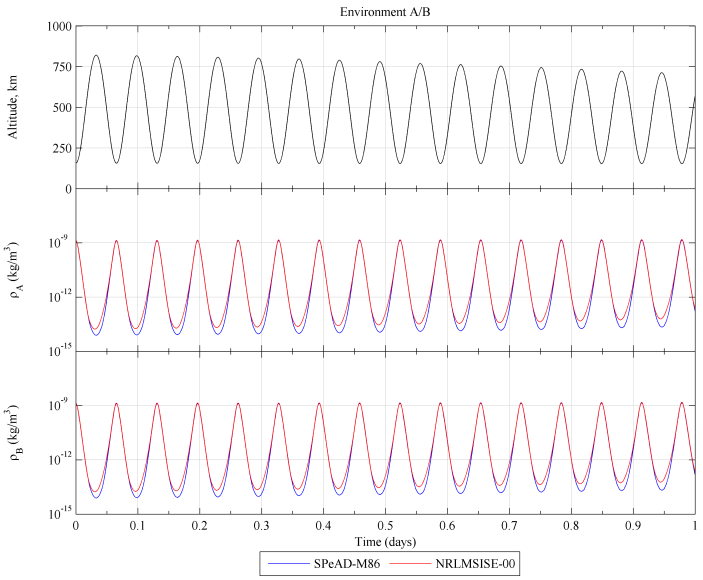

Figure 4. Density variations in Environments A and B with time; Δt = 0.1 second. Altitude data from NRLMSISE-00 implementation in Environment A.

Figure 4 presents the density variations for Environments A and B, alongside altitude data from the NRLMSISE-00 implementation in Environment A. This environment is considered the most accurate representation of the orbit and attitude dynamics, as it includes perturbation effects due to spherical gravitational harmonics. The variation in altitude over the course of an orbit significantly affects the atmospheric density which the spacecraft experiences during an orbit, as seen in Figure 4. Over one orbit, the density varies by five orders of magnitude, from 10^{-9} to 10^{-14} kg/m^3. The SPeAD-M86 model slightly under-predicts the density at higher altitudes, resulting in the a, e and ν errors. This underprediction is a result of the SPeAD-M86 model not accounting for the interaction of solar flux and geomagnetic field with the upper atmosphere. Over the simulation time of one day, the apogee is reduced from 843.9 km to 712.2 km, while the perigee is reduced from 156.1 km to 153.0 km. Figure 5 presents the density variations for Environments C and D alongside altitude data from the NRLMSISE-00 implementation in Environment C.

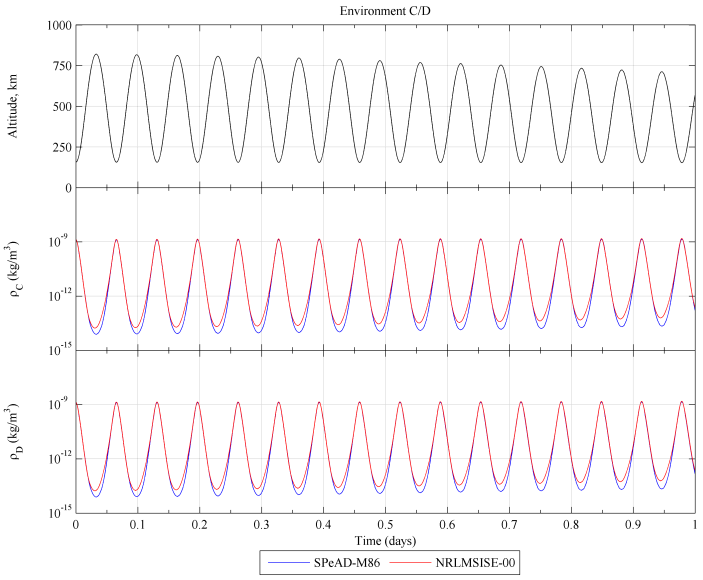

Figure 5. Density variations in Environments C and D with time; Δt = 1.0 second. Altitude data from NRLMSISE-00 implementation in Environment C.

From Figure 5, the apogee is reduced from 843.9 km to 711.7 km, while the perigee is reduced from 156.1

km to 153.0 km. The results are similar to those presented in Figure 4, with the SPeAD-M86 model slightly underpredicting the density at altitudes above 500 km. The increased Δt in Environments C and D does not appear to significantly affect the orbit propagation, indicating the results are independent of the time steps considered in this study. Figure 6 presents the orbital element error for Environment B.

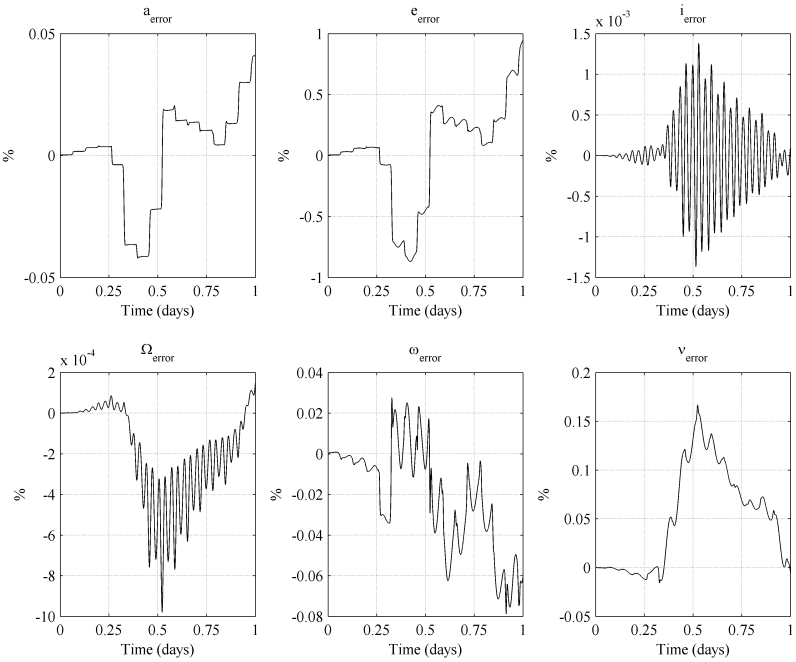

Figure 6. Environment B: Orbital element error between SPeAD-M86 and NRLMSISE-00 implementation.

Figure 6 illustrates that the errors in a, e, and ν are slightly larger than those observed for Environment A. However, all orbital element errors are less than 1% over the entire simulation period. The oscillatory nature of errors in i and Ω is visible, along with an interesting trend showing the error in ν increasing up to a maximum of 0.16% and then decreasing. Figure 7 presents the orbital element error for Environment C.

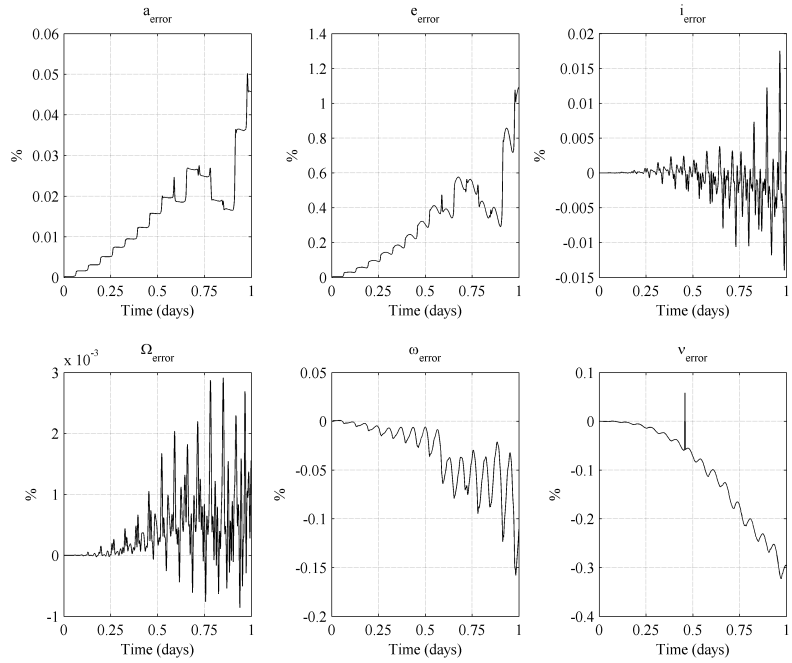

Figure 7. Environment C: Orbital element error between SPeAD-M86 and NRLMSISE-00 implementation.

Trends similar to those presented for Environment A and B are observed. However, a key distinction is the increase in i_{error} by an order of magnitude as compared to Environment A. In addition, the eccentricity error peaks at just over 1%. The spike in ν_{error} at ≈ 0.5 days is likely an anomaly caused by intermittent sensitivity of the propagation model to the time step, and does not affect the overall trend. Ω and i demonstrate oscillatory increasing errors. The underprediction of density presented in Figures 4 and 5 effectively reduces the circularization rate of the orbit as compared to the NRLMSISE-00 model, resulting in the positive error in e. The orbital element errors for Environment D are presented in Figure 7.

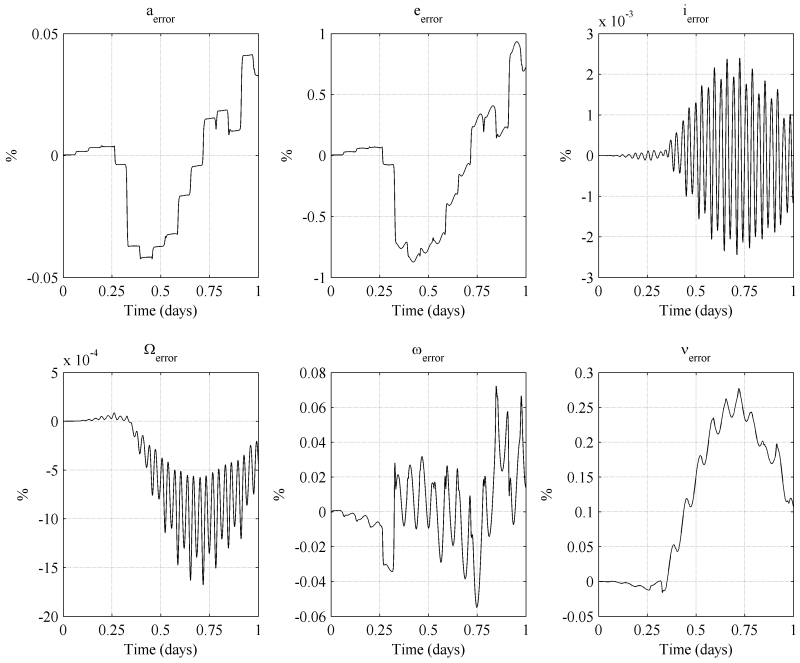

Figure 8. Environment D: Orbital element error between SPeAD-M86 and NRLMSISE-00 implementation.

Being the simplest and least computationally demanding simulation, Environment D was expected to exhibit the greatest effect on the accuracy of the SPeAD-M86 model. However, the results are similar to the values and trends presented for Environment B. The ability to propagate the orbit with reasonable accuracy while using a simplified simulation environment and a large time step verifies the stability of the SPeAD-M86 model.

V.C. CPU Run-time

In addition to examining the accuracy and sensitivity of the SPeAD-M86 model to orbit propagation environments, it was important to compare the CPU run time against a NRLMSISE-00 baseline. These results are summarized in Table 2.

Environment	Atmospheric Model	Average Run Time (sec)	Run Time Difference
A	NRLMSISE-00	244.9	↓ 27.6%
	SPeAD-M86	177.2	
B	NRLMSISE-00	174.8	↓ 18.5%
	SPeAD-M86	142.8	
C	NRLMSISE-00	26.83	↓ 27.0%
	SPeAD-M86	19.58	
D	NRLMSISE-00	18.52	↓ 17.2%
	SPeAD-M86	15.33	

Table 2: Simulation CPU Run Times

For all four environments, the use of the SPeAD-M86 model results in a substantial decrease in run time over the NRLMSISE-00 model, ranging from 17.2% to 27.6%. The effect is particularly significant in Environments A and C, indicating that use of SPeAD-M86 model in high fidelity simulation environments could prove particularly beneficial. Furthermore, the run-time reduction appears to be independent of the simulation time step. Results indicate that Environments B and D, which were designed to be computationally less require an average of 25% percent less CPU run-time compared to Environments A and C.

VI. Conclusion

In this work, based on a piece-wise exponential approach, a low computation atmospheric density model for CubeSat applications was developed and validated. Unlike existing atmospheric models, SPeAD-M86 presents a one-to-one relation between altitude and density for altitudes between 0 and 1000 km based on previously published empirical data. The proposed density correlation closely agrees with data from previously published empirical models. Propagation of spacecraft orbit and attitude agrees closely with a NRLMSISE-00 baseline, thus establishing the stability and validity of the SPeAD-M86 model. Furthermore, the proposed model reduces CPU run time by up to 27%, while maintaining a daily propagation error of less than 1% as compared with the NRLMSISE-00 model, thus making it suitable for orbit and attitude propagation on board low-computational space platforms such as CubeSats.

Future work on this model could include calibration against the MSIS-86 minimum and maximum $F_{10.7}$ density estimates. These additional lookup tables could potentially provide the model with the capability of accounting for the sinusoidal temporal variation of the solar flux within each solar cycle. An analogous sinusoidal correlation for geomagnetic activity could also improve the accuracy of the model.

Appendix

Altitude Interval, km	Scale Height, km	CIRA72 Base Density, kg/m^3
0 - 25	7.249	1.225E+00
25 - 30	6.349	3.899E-02
30 - 40	6.682	1.774E-02
40 - 50	7.554	3.972E-03
50 - 60	8.382	1.057E-03
60 - 70	7.714	3.206E-03
70 - 80	6.549	8.770E-05
80 - 90	5.799	1.905E-05
90 - 100	5.382	3.396E-06
100 - 110	5.877	5.297E-07
110 - 120	7.263	9.661E-08
120 - 130	9.473	2.438E-08
130 - 140	12.636	8.484E-09
140 - 150	16.149	3.845E-09
150 - 180	22.523	2.070E-09
180 - 200	29.74	5.464E-10
200 - 250	37.105	2.789E-10
250 - 300	45.546	7.248E-11
300 - 350	53.628	2.418E-11
350 - 400	53.298	9.518E-12
400 - 450	58.515	3.725E-12
450 - 500	60.828	1.585E-12
500 - 600	63.822	6.967E-13
600 - 700	71.835	1.454E-13
700 - 800	88.667	3.614E-14
800 - 900	124.64	1.170E-14
900 - 1000	181.05	5.245E-15

Table 3: CIRA72 Altitude Interval Data[13]

Altitude Interval, km	Scale Height, km	MSIS-86 Base Density, kg/m^3	Scale Density, kg/m^3
0 - 100	6.7	1.225	1.225
100 - 150	9.5	4.79E-07	1.30E-02
150 - 200	25.5	1.81E-09	5.70E-07
200 - 250	37.5	2.53E-10	4.80E-08
250 - 300	44.8	6.24E-11	1.60E-08
300 - 350	50.3	1.95E-11	7.40E-09
350 - 400	54.8	6.98E-12	4.00E-09
400 - 450	58.2	2.72E-12	2.60E-09
450 - 500	61.3	1.13E-12	1.70E-09
500 - 550	64.5	4.89E-13	1.10E-09
550 - 600	68.7	2.21E-13	6.30E-10
600 - 650	74.8	1.04E-13	3.10E-10
650 - 700	84.4	5.15E-14	1.10E-10
700 - 750	99.3	2.72E-14	3.00E-11
750 - 800	121	1.55E-14	7.10E-12
800 - 850	151	9.63E-15	1.90E-12
850 - 900	188	6.47E-15	5.90E-13
900 - 950	226	4.66E-15	2.40E-13
950 - 1000	263	3.54E-15	1.30E-13

Table 4: MSIS-86 Altitude Interval Data

The Matlab code for computing ν_{error} is presented below.

```
for i = 1:length(time)
v_error_temp =  COE_SP(i,6) - COE_NRL(i,6);
    if  v_error_temp > pi
        v_error_temp =  2*pi - (COE_SP(i,6) - COE_NRL(i,6));
    elseif v_error_temp < - pi
        v_error_temp =  2*pi + (COE_SP(i,6) - COE_NRL(i,6));
    else
    end
    v_error = [v_error (100/(2*pi))*v_error_temp];
end
```

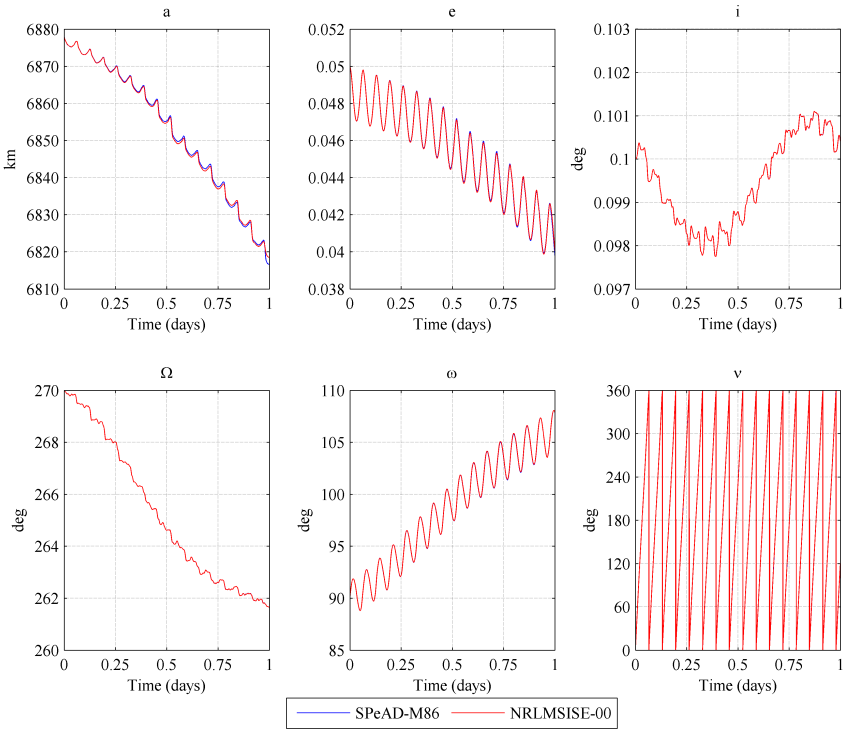

Figure 9. Environment A: Variation of orbital elements.

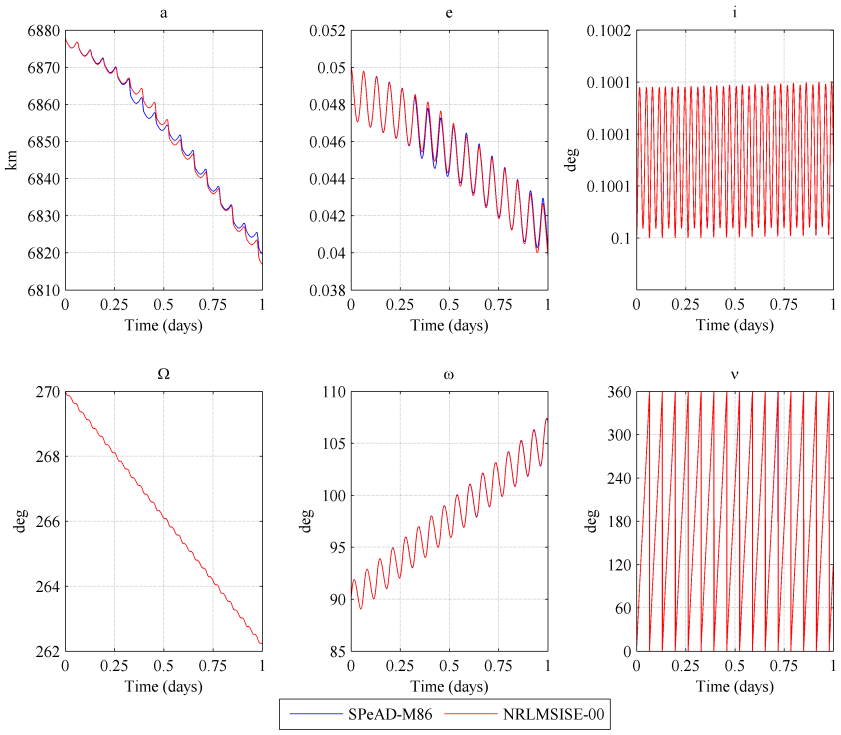

Figure 10. Environment B: Variation of orbital elements.

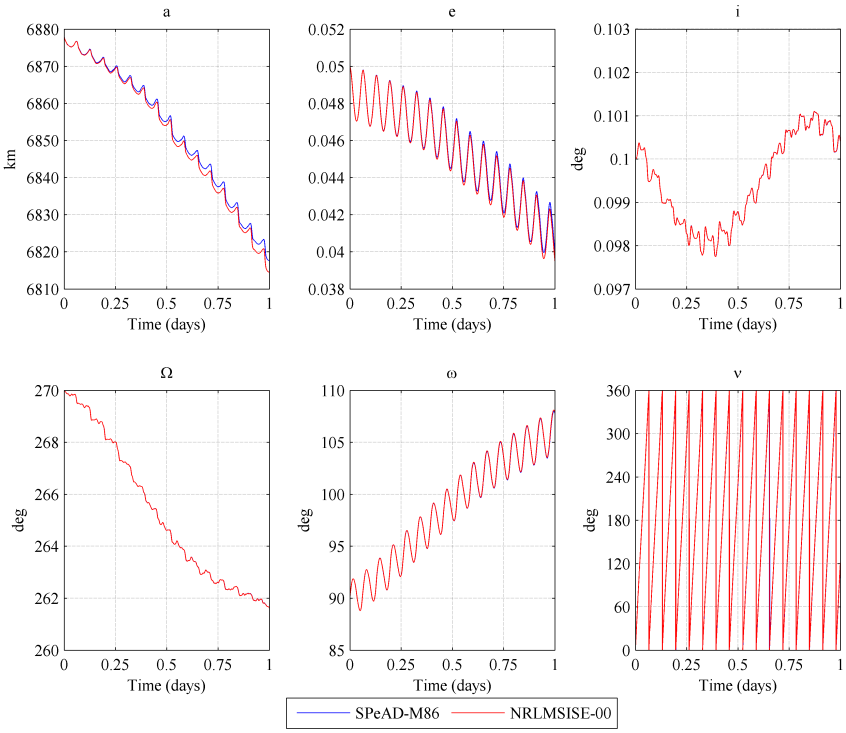

Figure 11. Environment C: Variation of orbital elements.

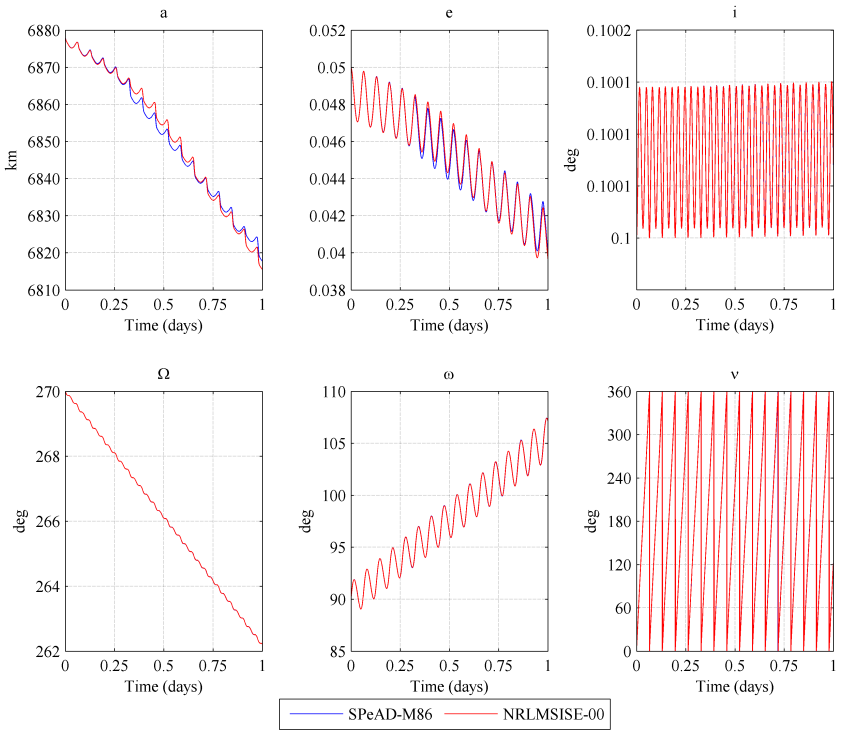

Figure 12. Environment D: Variation of orbital elements.

Acknowledgments

Mr. Kedare would like to graciously acknowledge Mr. Jonathan Kozich from Embry-Riddle Aeronautical University for his enlightening discussions and valuable feedback regarding the presentation of data within this paper.

References

[1]Surrey Satellite Technology Limited, *STRaND-1 Smartphone Nanosatellite*, 2014 (accessed May 6, 2014), http://www.sstl.co.uk/Missions/STRaND-1--Launched-2013/STRaND-1/STRaND-1--Smartphone-nanosatellite.

[2]Hall, L. and Dunbar, B., *Small Spacecraft Technology Program*, 2014 (accessed May 15, 2014), http://www.nasa.gov/directorates/spacetech/small_spacecraft/#.U4KVjPldXXQ.

[3]CubeSatShop.com, *ISIS On Board Computer*, 2014 (accessed May 26, 2014), http://www.cubesatshop.com/index.php?page=shop.product_details&flypage=flypage.tpl&product_id=119&category_id=8&option=com_virtuemart&Itemid=75.

[4]Bowen, J. A., *On-board Orbit Determination and 3-axis Attitude Determination for Picosatellite Applications*, Master's thesis, California Polytechnic State University, San Luis Obispo, California, 2009.

[5]Montenbruck, O. and Gill, E., *Satellite Orbits: Models, Methods, Applications*, Springer-Verlag, Berlin, 2000.

[6]Bate, R. R., Mueller, D. D., and White, J. E., *Fundamentals of Astrodynamics*, Dover Pulications, Inc., New York, 1971.

[7]Wertz, J. R., and Larson, W. J., *Space Mission Analysis and Design, 2nd ed.*, Microcosm and Springer, Hawthorne, CA, 2008.

[8]Tribble, A. C., *The Space Environment: Implications for Spacecraft Design*, Princeton University Press, Princeton, New Jersey, 2003.

[9]King-Hele, D., *Satellite Orbits in an Atmosphere*, Springer, 1st ed., 1987.

[10]Gaposchkin, E. M., "Calculation of Satellite Drag Coefficients," Tech. Rep. 998, MIT Lincoln Laboratory, MA, 1994.

[11]Vallado, D. A., and Finkelman, D., "A critical assessment of satellite drag and atmospheric density modeling," *Acta Astronautica*, Vol. 92, Feb. - March 2014, pp. 141–165.

[12]Champion, K. S. W., Cole, A. E., and Kantor, A. J., *Handbook of Geophysics and the Space Environment: Chapter 14*, National Technical Information Service, Springfield, VA, 1985, Document Accession Number: ADA 167000.

[13]Vallado, D. A. and McClain, W. D., *Fundamentals of Astrodynamics and Applications, 4th ed.*, Microcosm Press, Hawthorne, CA, 2013.

[14]Walter, U., *Astronautics: The Physics of Space Flight, 2nd ed.*, Wiley-VCH, Weinheim, Germany, 2012.

[15]Jacchia, L. G., "Revised Static Models for the Thermosphere and Exosphere with Empirical Temperature Profiles," *SAO Special Report No. 332*, Smithsonian Institution Astrophysical Observatory, Cambridge, MA, 1971.

[16]Roberts Jr., C. E., "An Analytic Model for Upper Atmosphere Densities Based upon Jacchias 1970 Models," *Celestial Mechanics*, Vol. 4, No. 3-4, December 1971, pp. 368–377.

[17]COSPAR Working Group IV, *COSPAR International Reference Atmosphere*, Akademie-Verlag, Berlin, 1972.

[18]National Technical Information Service, *U.S. Standard Atmosphere*, Springfield, Virginia, 1976, Product Number: ADA-035-6000.

[19]Bowman, B. R., Tobiska, W. K, Marcos, F., and Huang, C., "The Thermospheric Density Model JB2008 using New EUV Solar and Geomagnetic Indices," *37th COSPAR Scientific Assembly*, Annapolis, MD, July 1320 2008, p. 367, Symposium C, session 42 (oral). Paper number: C42-0004-08.

[20]Hedin, A. E. and Salah, J. E. and Evans, J. V. and Reber, C. A. and Newton, G. P. and Spencer, N. W. and Kayser, D. C. and Alcayde, D. and Bauer, P. and Cogger, L. and McClure J. P., "A Global Thermospheric Model Based on Mass Spectrometer and Incoherent Scatter Data," *Journal of Geophysical Research*, Vol. 82, 1977, pp. 2139–2156.

[21]Hedin, A. E., "Extension of the MSIS Thermosphere Model into the Middle and Lower Atmosphere," *Journal of Geophysical Research*, Vol. 96, 1991, pp. 1159–1172.

[22]Picone, J. M., Hedin, A. E., Drob, D. P. and A. C. Aikin, "NRLMSISE-00 Empirical Model of the Atmosphere: Statistical Comparisons and Scientific Issues," *Journal of Geophysical Research*, Vol. 107, No. A12, 2002.

[23]Akins, A., Healy, L., Coffey, S., and Picone, M. , "Comparison of MSIS and Jacchia Atmospheric Density Models for Orbit Determination and Propagation," *13th AAS/AIAA Space Flight Mechanics Meeting*, Ponce, Puerto Rico, February 9-13 2003, Paper AAS 03-165.

[24]Tewari, A., *Atmospheric and Space Flight Dynamics: Modeling and Simulation with MATLAB and Simulink*, Birkhauser, Boston, 2007.

[25]COSPAR Working Group, *COSPAR International Reference Atmosphere - 2012 Version: 1.0*, 2012 (accessed May 12, 2014), http://sol.spacenvironment.net/CIRA-2012.

[26]Picone, J. M., Drob, D. P., Meier, R. R., and Hedin, A. E., "NRLMSISE-00: A New Empirical Model of the Atmosphere," *NRL Review*, 2003, http://www.nrl.navy.mil/research/nrl-review/2003/atmospheric-science/picone/.

[27]Whitmore, S. A., "Closed-form integrator for the quaternion (euler angle) kinematics equations," May 9 2000, US Patent 6,061,611.

[28]NOAA, *NOAA National Geophysical Data Center FTP Site*, 2014 (accessed May 26, 2014), ftp://ftp.ngdc.noaa.gov/STP/GEOMAGNETIC_DATA/INDICES/KP_AP/2007.

[29]NorthWest Research Associates, Inc. Space Weather Services, *10.7 cm Solar Radio Flux*, 2014 (accessed May 15, 2014), http://www.nwra.com/spawx/f10.html.